Noname manuscript No.
(will be inserted by the editor)

Interactive multilevel focus+context visualization framework

Mahmudul Hasan · Faramarz F. Samavati · Christian Jacob

Received: date / Accepted: date

Abstract In this article, we present the construction of an interactive multilevel focus+context visualization framework for the navigation and exploration of large-scale 2D and 3D images. The presented framework utilizes a *balanced multiresolution* (BMR) technique supported by a *balanced wavelet transform* (BWT). It extends the mode of focus+context visualization, where spatially separate magnification of *regions of interest* (ROIs) is performed, as opposed to in-place magnification. Each resulting visualization scenario resembles a tree structure, where the root constitutes the main context, each non-root internal node plays the dual roles of both focus and context, and each leaf solely represents a focus. Our developed prototype supports interactive manipulation of the visualization hierarchy, such as addition and deletion of ROIs and desired changes in their resolutions at any level of the hierarchy on the fly. We describe the underlying data structure to efficiently support such operations. Changes in the spatial locations of query windows defining the ROIs trigger on-demand reconstruction queries. We explain in detail how to efficiently process such reconstruction queries within the hierarchy of *details* (wavelet coefficients) contained in the BWT in order to ensure real-time feedback. As the BWT need only be constructed once in a preprocessing phase on the server-side and robust on-demand reconstruction queries require minimal data communication overhead, our presented framework is a suitable candidate for efficient web-based visualization of complex large-scale imagery. We also discuss the performance characteristics of our proposed framework from various aspects, such as time and space complexities and achieved frame rates.

Keywords Focus+context visualization · Contextual close-up · Multilevel hierarchy · Balanced decomposition · Perfect reconstruction · Balanced wavelet transform

M. Hasan*(✉) · F. F. Samavati† · C. Jacob‡
*†‡Department of Computer Science
‡Department of Biochemistry & Molecular Biology
University of Calgary, Calgary, Alberta, Canada
e-mail: mhasan@ucalgary.ca

1 Introduction

The continuous growth of 2D/3D image size in various application domains and the prolific use of handheld devices mandate the ability to visualize and explore large-scale images within the physical and ergonomic limitations of the screen space available on such devices. To address this issue, in this article, we present a multilevel focus+context visualization framework for large-scale 2D and 3D images. The advantages of such a visualization framework are manifold. It allows for more manageable utilization of screen space by the creation of a multilevel visualization hierarchy. In such a multilevel hierarchy, enlarged *regions of interest* (ROIs) can also serve as contexts to further increase the depth of the hierarchy, if required. Therefore, such a hierarchy permits the visualization of contexts with higher *degrees of interest* [3] in higher resolutions, while maintaining interactive frame rates. The ability to have multiple ROIs at different desired resolutions also enables users to draw comparisons between ROIs when applicable.

Query window-based focus+context visualization is useful for the visualization and exploration of large-scale 2D and 3D images. It allows simultaneous visualization of both the local and global views of the data, possibly at varying scales. Facilitating such visualization involves rendering a low-resolution approximation of data providing the context and a high-resolution approximation

of an enclosed ROI selected by a query window, defining the focus. The work presented in this article extends this mode of focus+context visualization to construct a multilevel focus+context visualization framework.

Such a visualization framework can be supported by a multiresolution approach, allowing different levels of detail of the data to be properly retrieved, scaled, and rendered at different resolutions on demand. Wavelet transform representations can be exploited to produce coarse approximations of data while retaining the ability to recover the original data when more detail is desired. This can enhance the overall visualization throughput by removing excessive details unless required. Additionally, wavelet transformation ensures a linear runtime for decomposition and reconstruction with no additional storage requirements.

In order to support the presented visualization framework by an underlying wavelet transform, on-demand reconstruction of high-resolution approximations of the ROIs from low-resolution approximations of data and their corresponding details (wavelet coefficients) is required. Here we exploit a *balanced wavelet transform* (BWT) by means of a *balanced multiresolution* (BMR) technique that provides efficient and straightforward access to details on demand [8]. The work presented in [8] allows the construction of BMR schemes for any set of regular multiresolution filters from the family of symmetric/antisymmetric filters that encompasses a wide range of commonly used filters. For decomposition and reconstruction purposes, the constructed BMR schemes use symmetric/antisymmetric extensions at image and detail boundaries. Notably, any such BMR scheme only makes use of regular multiresolution filters, completely eliminating the need for any extraordinary boundary filters.

Such a framework can be used to efficiently support web-based visualization and exploration of complex large-scale imagery on handheld devices with limited screen spaces. This is possible due to the BWT, which need only be constructed once (for each image) on the server-side in a preprocessing phase and allows robust on-demand reconstruction queries to be performed with minimal communication overhead using the *L-updating* technique described later in this article. Furthermore, *scalability and multilevel hierarchy* was highlighted as one of the top ten challenges regarding *interaction and user interfaces* in extreme-scale visual analytics by Wong *et al.* [26]. We envision that our presented framework for large-scale image visualization and exploration will provide insights toward developing similar visualization frameworks suitable for extreme-scale visual analytics.

Hasan *et al.* introduced multilevel focus+context visualization supported by balanced multiresolution [7]. In this article, we expand their work in several aspects. First, we improve the underlying data structure supporting the multilevel visualization hierarchy to reduce storage requirement. Second, we provide a generalized flowchart demonstrating the focus+context visualization pipeline of our proposed multilevel framework, which is independent of what multiresolution filters (see Section 4.1.1) are used and also gives a high-level guideline for a web-based implementation of our proposed framework. Furthermore, in addition to a new set of results exhibiting multilevel focus+context visualization scenarios for large-scale 2D and 3D images, we discuss the performance characteristics of our framework with respect to time and space complexities, achieved frame rates, and implications of using different sets of multiresolution filters.

The operations we specify for pixels in this article are readily applicable to voxels. So from this point forward, we generally refer to pixels and voxels as *samples*.

This article is organized as follows. In section 2, we present the notations used throughout the article for multiresolution operations. Next, a brief survey of related work follows in section 3. Section 4 presents the construction of our multilevel focus+context visualization framework. In section 5, we present the experimental results produced by our developed prototype, followed by an analysis of the performance characteristics of our proposed framework in Section 6. Section 7 concludes the article with directions for future work.

2 Notation

The article adopts and extends the notations for denoting multiresolution operations used by Samavati *et al.* in [20].

2.1 Decomposition

Given a column vector of fine samples C^k, a column vector of coarse samples C^{k-1} is obtained by downsampling C^k using the matrix equation

$$C^{k-1} = \mathbf{A}^k C^k, \tag{1}$$

and the *details* lost due to downsampling, denoted by D^{k-1} are captured using the matrix equation

$$D^{k-1} = \mathbf{B}^k C^k. \tag{2}$$

$\mathbf{A}^k$ and $\mathbf{B}^k$ used in equations (1) and (2) are decomposition (analysis) filter matrices. This process of deriving C^{k-1} and D^{k-1} from C^k is referred to as *decomposition*. Note that for image decomposition, the sequences

of samples along each dimension can be treated independently, allowing any such sequence to form C^k for decomposition.

2.2 Reconstruction

The *reconstruction* process involves recovering the column vector of fine samples C^k from the column vectors of coarse sample C^{k-1} and corresponding details D^{k-1}. Reconstruction (synthesis) filter matrices $\mathbf{P}^k$ and $\mathbf{Q}^k$ respectively refine C^{k-1} and D^{k-1} to recover C^k as follows:

$$C^k = \mathbf{P}^k C^{k-1} + \mathbf{Q}^k D^{k-1}. \tag{3}$$

Equation (3) reverses the application of decomposition filter matrices $\mathbf{A}^k$ and $\mathbf{B}^k$ on the original column vector of fine samples C^k. So decomposition and reconstruction are inverse processes that satisfy

$$\begin{bmatrix} \mathbf{A}^k \\ \mathbf{B}^k \end{bmatrix} \begin{bmatrix} \mathbf{P}^k & \mathbf{Q}^k \end{bmatrix} = \begin{bmatrix} \mathbf{I} & \mathbf{0} \\ \mathbf{0} & \mathbf{I} \end{bmatrix}.$$

2.3 Wavelet transform

Recursive decompositions of a column vector of fine samples C^k into column vectors of coarse samples

$$C^l, C^{l+1}, \ldots, C^{k-1}$$

and corresponding details

$$D^l, D^{l+1}, \ldots, D^{k-1}$$

construct the *wavelet transform* of C^k, denoted by

$$C^l, D^l, D^{l+1}, \ldots, D^{k-1},$$

where $l < k$. From this wavelet transform, we can fully or partially reconstruct each of $C^{l+1}, \ldots, C^{k-1}, C^k$.

2.4 Simplified notations

For the rest of the article, we simplify the notations by omitting the superscript k for the kth level of resolution with the following assumptions: $F = C^k$, $C = C^{k-1}$, $D = D^{k-1}$, $\mathbf{A} = \mathbf{A}^k$, and $\mathbf{B} = \mathbf{B}^k$, $\mathbf{P} = \mathbf{P}^k$, and $\mathbf{Q} = \mathbf{Q}^k$. Also, the decomposition and reconstruction filter matrices are assumed to have appropriate sizes to satisfy the equations

$$C = \mathbf{A}F, \tag{4}$$
$$D = \mathbf{B}F, \tag{5}$$
$$F = \mathbf{P}C + \mathbf{Q}D. \tag{6}$$

The filter matrices $\mathbf{A}$, $\mathbf{B}$, $\mathbf{P}$ and $\mathbf{Q}$ we consider are of banded, repetitive, and slanted structure. So, let the nonzero entries in a representative row of $\mathbf{A}$ and $\mathbf{B}$ be represented by decomposition filter vectors $\mathbf{a}$ and $\mathbf{b}$, respectively. In a similar manner, let the nonzero entries in a representative column of $\mathbf{P}$ and $\mathbf{Q}$ be denoted by reconstruction filter vectors $\mathbf{p}$ and $\mathbf{q}$, respectively.

3 Background literature

The following two subsections present a brief review of existing related work on multiresolution and focus+context visualization.

3.1 Multiresolution

Due to the regular structure of images, multiresolution methods applicable to curves and regular meshes (tensor-product surfaces and volumes) are also applicable to images. A mathematically clean and efficient approach to multiresolution based on reverse subdivision was made possible due to the work of Samavati and Bartels [1,2,19]. For decomposition, their approach involves obtaining each coarse vertex through an efficient local least squares optimization, which reduces undesired undulations. Furthermore, compared to the conventional wavelets for curves and regular surfaces, the wavelets resulting from this approach provide a more compact support. The multiresolution filters we used to produce the experimental results in section 5 were derived using this approach.

Conventional multiresolution schemes for the local filters of second or higher order scaling functions and their wavelets lead to unequal numbers of coarse and detail samples after decomposition. This inequality makes locating the details required for the on-demand reconstruction of an enlarged ROI in a multilevel visualization hierarchy cumbersome. Furthermore, such multiresolution schemes may need to use extraordinary boundary filters in order to handle image and detail boundaries. This makes the reconstruction of ROI sub-regions near image boundaries computationally untidy. In order to address these issues, Hasan *et al.* recently introduced a technique for devising BMR schemes for a class of multiresolution filter vectors that are symmetric/antisymmetric about their centers [8].

The use of a wavelet tree [24], octree-based hierarchies [13,17,21], and resampling based on space deformation [25] are noteworthy existing approaches supporting context-aware multiresolution visualization of 3D images. The wavelet-based time-space partitioning (WTSP) tree was utilized for 4D images in [24]. In order to support

context-aware multiresolution visualization of a 2D or 3D image, we construct its BWT as suggested in [8], which compactly stores a coarse approximation of the image in addition to a hierarchy of details (see Fig. 1, for example).

3.2 Focus+context visualization

Hauser generalized focus+context visualization across the fields of information and scientific visualizations based on the various methods (such as graphics resource allocation) used to discriminate between data subsets corresponding to focus and context [9]. Using a metaphor of lenses is a prominent way of supporting focus+context visualization [11, 22, 25]. This technique is influenced by traditional handcrafted medical, technical, and scientific illustrations [10]. According to the categorization by Cohen and Brodlie [5], our implemented multiresolution approach to this metaphor of lenses is discontinuous and undistorted like that in [22], as opposed to continuous and distorted techniques in [11, 25].

Multifocal and/or multicontext visualization techniques have been used in the literature for various types of data. Cossalter *et al.* used a multifocal multilevel technique for network visualizations [6]. Tu and Shen presented a multifocal technique applicable to treemap visualizations for hierarchical data [23]. Mendez *et al.* used a multifocal [15] and Kalkofen *et al.* a multicontext [12] approach to focus+context visualization in augmented reality applications. Ropinski *et al.* made use of a multifocal approach, utilizing multiple interactive closeups for the visualization of multiple modalities of medical data [18]. Packer presented a technique for illustrative multifocal multicontext visualization of layered tubular volumes (for instance, human muscle tissue) along a snaking path in a perspective view [16]. In contrast to this body of work, we take a multiresolution approach to interactive multilevel focus+context visualization, supported by an underlying BWT.

4 Methodology

We support our multilevel focus+context visualization framework using an underlying BWT constructed by a BMR scheme for two reasons. Firstly, a BWT provides straightforward access to details corresponding to a ROI in a multilevel hierarchy. Secondly, a BMR scheme does not require any extraordinary boundary filters, the use of which leads to computationally untidy reconstruction of ROI sub-regions near image boundaries. Additionally, we present an efficient technique for processing reconstruction queries to ensure real-time feedback and a sample normalization and quantization method we adopted for rendering purposes.

4.1 Balanced multiresolution (BMR)

We utilize a BMR scheme devised according to the construction procedure presented in [8]. Using a given set of regular multiresolution filter vectors **a**, **b**, **p**, and **q** that are symmetric/asymmetric in structure, a BMR scheme allows for a balanced decomposition and a subsequent perfect reconstruction of a dataset. Here, balanced decomposition is defined such that $size(C) = size(D) = size(F)/2$, where $size(\ldots)$ returns the number of elements in the argument vector.

A BMR scheme avoids the use of extraordinary boundary filters using an extended version of the column vector of fine samples F for decomposition and, similarly, extended versions of the column vectors of coarse samples C and detail samples D for reconstruction. Let F' denote the extended version of F, obtained through symmetric extensions at the boundaries. Also, let C' and D' denote the extended versions of C and D, respectively, obtained through symmetric/antisymmetric extensions at their boundaries. Then the decomposition and reconstruction processes of a BMR scheme are governed by the equations

$$C = \mathbf{A}F', \tag{7}$$

$$D = \mathbf{B}F', \tag{8}$$

$$F = \mathbf{P}C' + \mathbf{Q}D', \tag{9}$$

analogous to equations (4), (5), and (6), respectively.

4.1.1 Multiresolution filters

The BMR scheme we use is devised using the *short* local filters of quadratic (third order) B-spline:

$$\begin{cases} \mathbf{a} = \begin{bmatrix} a_{-2} & a_{-1} & a_1 & a_2 \end{bmatrix} = \begin{bmatrix} -\frac{1}{4} & \frac{3}{4} & \frac{3}{4} & -\frac{1}{4} \end{bmatrix}, \\ \mathbf{b} = \begin{bmatrix} b_{-2} & b_{-1} & b_1 & b_2 \end{bmatrix} = \begin{bmatrix} \frac{1}{4} & -\frac{3}{4} & \frac{3}{4} & -\frac{1}{4} \end{bmatrix}, \\ \mathbf{p} = \begin{bmatrix} p_{-2} & p_{-1} & p_1 & p_2 \end{bmatrix} = \begin{bmatrix} \frac{1}{4} & \frac{3}{4} & \frac{3}{4} & \frac{1}{4} \end{bmatrix}, \\ \mathbf{q} = \begin{bmatrix} q_{-2} & q_{-1} & q_1 & q_2 \end{bmatrix} = \begin{bmatrix} -\frac{1}{4} & -\frac{3}{4} & \frac{3}{4} & \frac{1}{4} \end{bmatrix}. \end{cases} \tag{10}$$

The filter vectors in (10) were constructed by reversing Chaikin subdivision [4] in [20]. Note that they are symmetric/antisymmetric about their centers, as required for setting up a BMR scheme.

4.1.2 Balanced decomposition

Following the general construction for a balanced decomposition in [8], for a column vector of fine samples

$F = [f_1\ f_2\ \ldots\ f_{2n}]^T$ where $n \in \mathbb{Z}^+$, we obtain

$F' = [f_1\ f_1\ \ldots\ f_{2n}\ f_{2n}]^T$

through half-sample symmetric extensions at the two boundaries of F. Then the column vectors of coarse samples $C = [c_1\ c_2\ \ldots\ c_n]^T$ and detail samples $D = [d_1\ d_2\ \ldots\ d_n]^T$ are obtained as follows:

$$\begin{cases} c_1 &= a_{-2}f_1 + a_{-1}f_1 + a_1 f_2 + a_2 f_3, \\ d_1 &= b_{-2}f_1 + b_{-1}f_1 + b_1 f_2 + b_2 f_3, \\ \vdots & \\ c_i &= a_{-2}f_{2i-2} + a_{-1}f_{2i-1} + a_1 f_{2i} + a_2 f_{2i+1}, \\ d_i &= b_{-2}f_{2i-2} + b_{-1}f_{2i-1} + b_1 f_{2i} + b_2 f_{2i+1}, \\ \vdots & \\ c_n &= a_{-2}f_{2n-2} + a_{-1}f_{2n-1} + a_1 f_{2n} + a_2 f_{2n}, \\ d_n &= b_{-2}f_{2n-2} + b_{-1}f_{2n-1} + b_1 f_{2n} + b_2 f_{2n}, \end{cases} \tag{11}$$

for $i = 2 \ldots (n-1)$. Note that (11) shows a linear evaluation of C and D using matrix equations (7) and (8), respectively.

Balanced decomposition along one or more dimensions of an image for a desired number of levels creates the corresponding BWT. For the purpose of demonstration, Fig. 1 shows the BWT resulting after two levels of heightwise and widthwise balanced decompositions of a 1024×512 Blue Marble image (data source: Visible Earth, NASA). Note that in practice, images that require multilevel focus+context visualization are larger in size.

4.1.3 Perfect reconstruction

According to the general construction for a perfect reconstruction provided in [8], we obtain

$C' = [c_1\ c_1\ \ldots\ c_n\ c_n]^T$

using half-sample symmetric extensions at the two boundaries of C and

$D' = [-d_1\ d_1\ \ldots\ d_n\ -d_n]^T$

using half-sample antisymmetric extensions at the two boundaries of D. Then the column vector of fine samples F is reconstructed from C' and D' as follows:

$$\begin{cases} f_1 &= p_2 c_1 + p_{-1}c_1 + q_2(-d_1) + q_{-1}d_1, \\ \vdots & \\ f_{2i} &= p_1 c_i + p_{-2}c_{i+1} + q_1 d_i + q_{-2}d_{i+1}, \\ f_{2i+1} &= p_2 c_i + p_{-1}c_{i+1} + q_2 d_i + q_{-1}d_{i+1}, \\ \vdots & \\ f_{2n} &= p_1 c_n + p_{-2}c_n + q_1 d_n + q_{-2}(-d_n), \end{cases} \tag{12}$$

for $i = 1 \ldots (n-1)$. Observe that (12) shows a linear evaluation of F using the matrix equation (9).

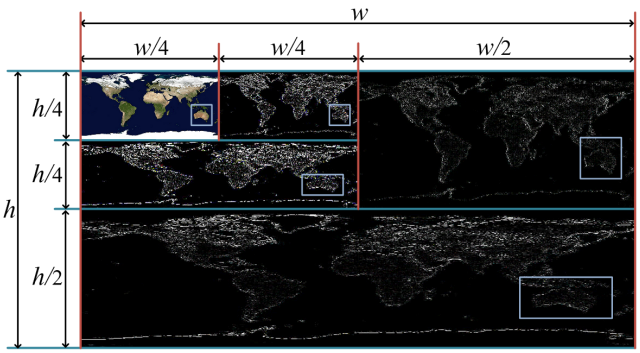

Fig. 1 BWT of a $w \times h$ Blue Marble image after two levels of balanced decomposition, with rectangles enclosing all levels of details corresponding to a ROI in the coarse approximation of the image (in the top-left corner). Source image dimensions: 1024×512. Figure adapted from [7]

4.2 Reconstruction queries

In this section, we focus on various aspects of efficiently processing on-demand reconstruction queries in a multilevel focus+context visualization framework.

4.2.1 On-demand access to details

For processing reconstruction queries in our multilevel focus+context visualization framework, we need to perform on-demand reconstruction of context sub-regions that define the ROIs from an underlying BWT. To do this, we need to locate the details corresponding to each ROI. Fig. 1 shows a ROI in the coarse approximation of an image and corresponding details contained within the BWT of a Blue Marble image. Regardless of what level of the visualization hierarchy a ROI is from, the balanced structure of the BWT makes locating the corresponding details straightforward. For instance, observe the reconstruction of interior samples in (12) — if the first coarse sample in the reconstruction of a fine sample is c_i, then d_i is the first detail sample to use in the reconstruction of that fine sample. Furthermore, that fine sample is either f_{2i} or f_{2i+1} depending on which reconstruction filters are used.

4.2.2 L-updating: avoiding redundant reconstructions

Depending on the depth of the multilevel visualization hierarchy where a moving query window (defining changing ROIs) is located, the triggered reconstruction queries can become computationally expensive. This negatively affects the ability to provide real-time feedback. To address this issue, here we describe an *L-updating* technique we employed to avoid redundant reconstruction

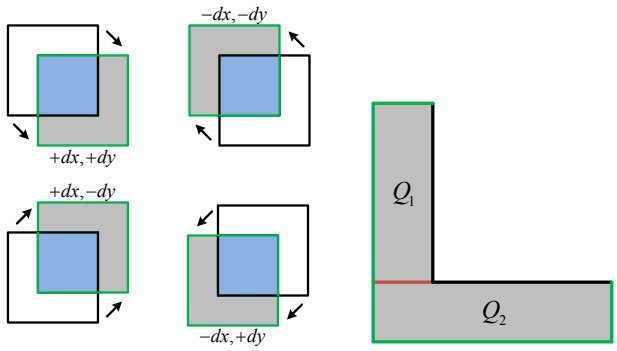

(a) L-updating scenarios (b) L-updating queries

Fig. 2 The L-updating technique. Figure adapted from [7]

operations. It works in a manner similar to clipmap-update for terrain rendering performed by Losasso and Hoppe, where they utilized L-like clip regions [14].

We explain the concept of L-updating for 2D images, which is extendable to work with 3D images in a straightforward manner. The ROI in a coarse approximation of a 2D image is identified by a movable rectangular query window. Fig. 2(a) shows four configurations of how such a query window can move. In each configuration, the rectangles with black and green edges represent the old and new locations of the query window before and after a move, respectively. The rectangular area shaded in light-blue represents the intersection between the old and new ROIs for each configuration. The signed dx and dy values represent the direction and magnitude of the move made by the query window.

In most scenarios, the old and new ROIs intersect. Provided that the high-resolution approximation of the old ROI has already been reconstructed, that for the intersection region (shown in light-blue for the each scenario in Fig. 2(a)) can be reused directly from the old enlarged ROI while obtaining the new enlarged ROI. Therefore, for each scenario, we only need to reconstruct the high-resolution approximation for the L-like polygonal area of the new ROI shaded in grey.

In order to reconstruct the high-resolution approximation for the L-like polygonal area of the new ROI, we break it down into two rectangular reconstruction queries, Q_1 and Q_2, as shown in Fig. 2(b). Note that if either dx or dy is zero, then there will be only one reconstruction query instead. From the standpoint of implementation, the same memory area can be used to update the high-resolution approximation of the old ROI into the high-resolution approximation of the new ROI. This process involves shifting the reusable high-resolution approximation of the old ROI to the opposite corner (observe in Fig. 2(a)) and copying the results of Q_1 and Q_2 to the appropriate locations.

The L-updating technique significantly reduces the computational overhead by eliminating redundant reconstruction operations. While exploiting a 3D query probe for interactive visualization and exploration of 3D images, utilizing the L-updating technique can result in a substantial gain in performance. It can also greatly minimize the data communication overheads in applications of our presented framework to web-based visualization and exploration of large-scale imagery.

4.3 Data structure

Supporting interactive manipulation of the multilevel focus+context visualization hierarchy mandates efficient hierarchy traversal capabilities of the underlying implementation. For example, addition and deletion of ROIs at any level of the hierarchy on the fly, changing the resolution of an enlarged ROI at some level in the hierarchy, and adjusting the visualization layout changing the locations of enlarged ROIs on the screen – they all require real-time traversal of the hierarchy. Therefore, we need to keep track of the tree-like structure of visualization scenarios supported by our presented framework.

Because a context window may contain any number of ROIs, each resulting visualization scenario resembles an N-ary tree structure (where each node has no more than N children). In order to allow for efficient traversal of the multilevel hierarchy on-demand and storage of pertinent information in a 1D array T, Hasan *et al.* made use of a *left-child right-sibling* (LC-RS) binary tree [7], corresponding to the N-ary tree that represents the layout of a visualization scenario. However, because t_{2i} and t_{2i+1} store the two children of the parent stored in t_i, the array T required $O(2^x)$ storage, where x is the maximum number of ROIs allowed in a visualization scenario. At any instance of time, only a maximum of x of the $O(2^x)$ array locations were useful.

In order to eliminate the waste of storage noted above, we exploit a linked list representation of the N-ary tree corresponding to a visualization scenario. Each node of the linked list contains a pointer to an object containing relevant ROI information and four additional pointers to the tree-nodes containing its parent, first-child, left-sibling, and right-sibling. The object containing ROI information stores the enlarged ROI for rendering and further reconstruction purposes, in addition to some pertaining information, such as its location in the main context, screen coordinates, etc. The main context, which is a part of the BWT, is not stored separately in such an object for reducing storage requirement.

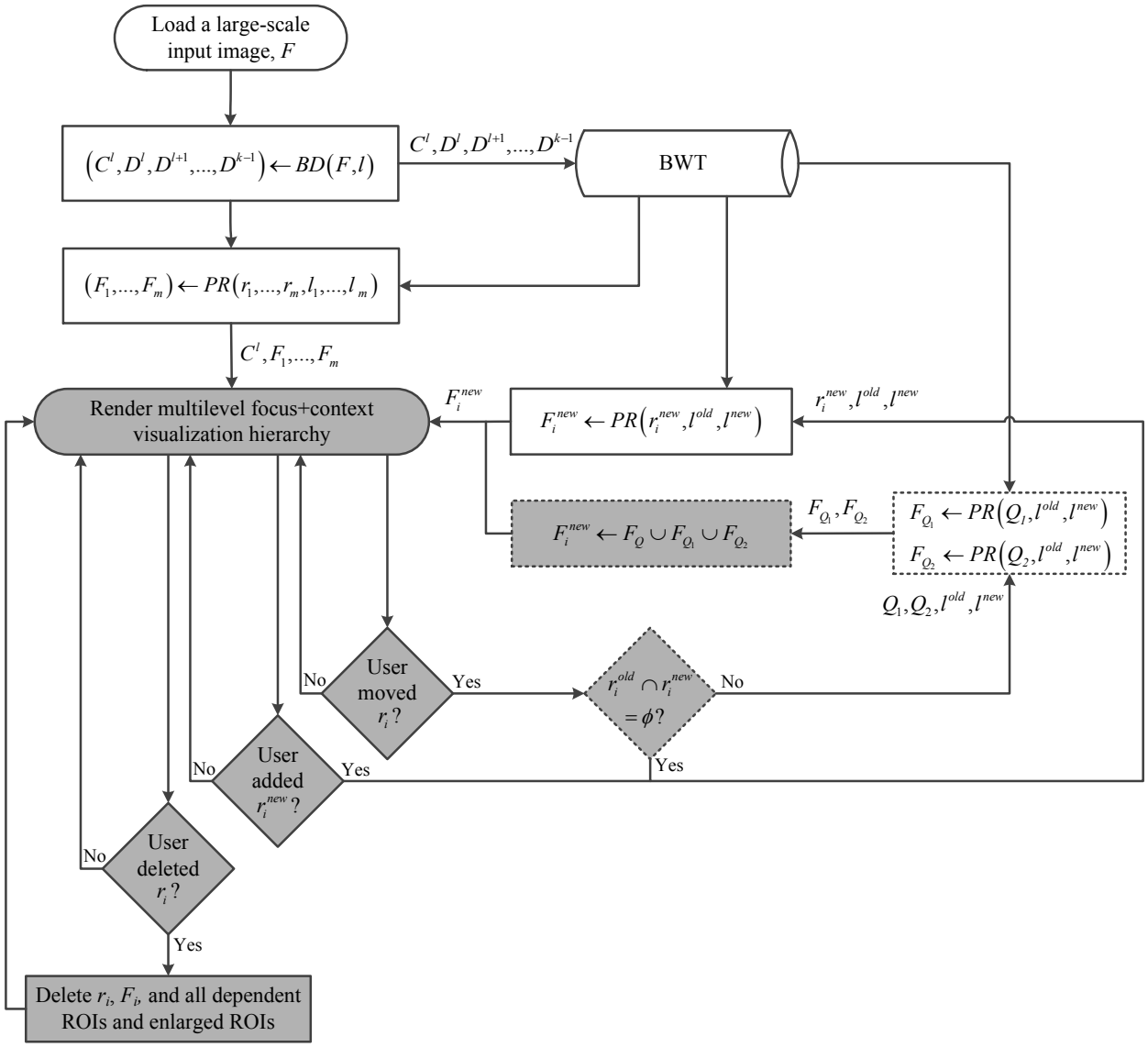

Fig. 3 Flowchart for the proposed multilevel focus+context visualization framework

4.4 Rendering: sample normalization and quantization

When a decomposition filter value is applied to a sample, it is applied independently to each of its components (such as red, green, and blue). The resulting sample will usually have each of its components as floating point values, which must be stored to ensure a perfect (lossless) reconstruction. These floating point values may also fall outside the interval of $[0, iMax]$, where $iMax$ is the maximum integer intensity value. However, for rendering purposes, these floating point values must be mapped to the integer range of 0 to $iMax$. A simple strategy for normalization is to replace the floating point values less than the minimum intensity of 0 with 0 and greater than the maximum intensity $iMax$ with $iMax$. Rounding up or down according to a preset criterion can quantize the floating point values between 0 and $iMax$. For the purpose of rendering, we obtain an integer intensity value i from a floating point value f as follows:

$$i = \begin{cases} 0 & \text{if } f \leq 0, \\ \lfloor f \rfloor & \text{if } 0 < f < iMax \wedge (f - \lfloor f \rfloor) \leq 0.5, \\ \lceil f \rceil & \text{if } 0 < f < iMax \wedge (f - \lfloor f \rfloor) > 0.5, \\ iMax & \text{if } f \geq iMax. \end{cases} \tag{13}$$

The experimental results provided in section 5 are rendered using the conditions in (13). Other commonly used approaches involve uniformly mapping either the pre-calculated possible interval or the actual interval of the resulting floating point values to the integer range of 0 to $iMax$. These approaches have varying impacts on the contrast of the resulting images.

One can avoid this normalization and quantization step by using multiresolution filters that map integer samples to integer samples. However, devising BMR schemes based on such multiresolution filters still remains unexplored.

4.5 Multilevel focus+context visualization framework

The high-level flowchart in Fig. 3 illustrates the pipeline and the important components of our proposed visualization framework. For simplification purposes, changes in existing ROIs' levels of resolution, modification of visualization hierarchy layout (relocating the enlarged ROIs on the screen), etc. supported by our developed prototype were not taken into consideration in this flowchart. In case of a web-based implementation, the grey components of this flowchart should to be performed on the client-side and the rest on the server-side. The three components with dashed borders constitute the L-updating technique described in Section 4.2.2. Several of the processes in this flowchart use the $BD(\ldots)$ and $PR(\ldots)$ methods to perform balance decomposition(s) and perfect reconstruction(s), respectively.

The first process loads a large-scale image F. In the second process, F undergoes l levels of balanced decomposition to construct the corresponding BWT (as defined in Sections 2.3 and 4.1.2). The following process relies on the constructed BWT to perfectly reconstruct the initial set of enlarged ROIs $F_1, ..., F_m$ with levels of resolution $l_1, ..., l_m$ based on the regions enclosed by the corresponding ROIs $r_1, ..., r_m$ in C^l, respectively. Then $C^l, F_1, ..., F_m$ are passed to the following process for rendering a multilevel focus+context visualization hierarchy. The visualization task may terminate at the end of this process.

Next, if the user moves a ROI r_i, and the old and new regions enclosed by r_i intersect, i.e. $r_i^{old} \cap r_i^{new} \neq \phi$, then Q_1 and Q_2 (as defined in Section 4.2.2) are passed to the following process with their current and expected levels of resolutions, l^{old} and l^{new}. Taking these, the following process perfectly reconstructs F_{Q_1} and F_{Q_2} relying on the BWT of image F. Provided F_{Q_1} and F_{Q_2}, the next process combines these to the reusable part of F_i (shaded in ligh-blue in Fig. 2), denoted by F_Q in the flowchart, to obtain F_i^{new}. F_i^{new} is then passed to the rendering process to update the previously rendered visualization hierarchy.

On the other hand, if the user moves a ROI r_i, and the old and new regions enclosed by r_i do not intersect, i.e. $r_i^{old} \cap r_i^{new} = \phi$, then F_i^{new} is perfectly reconstructed from r_i^{new}, l^{old}, l^{new} and the BWT by a different process as shown in the flowchart. The process also perfectly reconstructs an enlarged ROI F_i^{new} if the user adds a new ROI r_i^{new} at some level in the hierarchy. Conversely, if the user deletes a ROI r_i from some level in the hierarchy, then a process deletes r_i, it enlarged version F_i, and all dependent ROIs and enlarged ROIs.

5 Results

We have developed a visualization tool prototype to validate our presented multilevel focus+context visualization framework for images. In Figs. 4 and 5, the associated levels of decomposition and reconstruction are shown at the bottom-right corner of each main context and at the top-right corner of each enlarged ROI, respectively.

Fig. 4 shows several focus+context visualization and exploration scenarios for 2D images facilitated by our developed tool. Figures 4(a) and 4(b) present multilevel focus+context visualization of a diseased leaf (data source: S. Fraser-Smith, Wikipedia; used under the Creative Commons Attribution 2.0 Generic license) and the topography of Long Island (data source: G. Hanson, Stony Brook University, USA), respectively. Fig. 4(c) draws a comparison between the ice near the coasts of the Prince of Wales Island and the Alexander Island using a Blue Marble image showing Earth's topography and bathymetry (data source: Visible Earth, NASA). Our developed prototype also allows fractional changes in the resolution of an enlarged ROI through trilinear interpolation between two consecutive integer resolutions of the ROI; Fig. 4(d) shows such a ROI at floating point resolution 4.15, magnifying a thin section cut through a bone marrow area in the kneecap of a mouse (data source: Dartmouth College Electron Microscope Facility, USA).

Our prototype allows focus+context visualization and exploration of a 3D image by means of interactive depthwise transitions of query windows defining the ROIs. Such transitions are controlled by the user either through the use of the attached mouse scroll wheel or the up and down arrow keys on the attached keyboard. Currently, our prototype only performs widthwise and heightwise decompositions of 3D images, keeping the number of 2D slices along the depth constant for depthwise volume exploration. Fig. 5 presents such a visualization scenario created in our prototype. For the sake of demonstration, it only shows the fly-through transition of two query windows through ten of the 150 sequential slices loaded into our prototype for this visualization task. The dimensions of the original dataset are $1056 \times 1528 \times 1477$ (data source: Male head, The Visible Human Project, U.S. National Library of Medicine). In a similar manner, our developed prototype can also process large-scale time-lapse imagery, constraining the

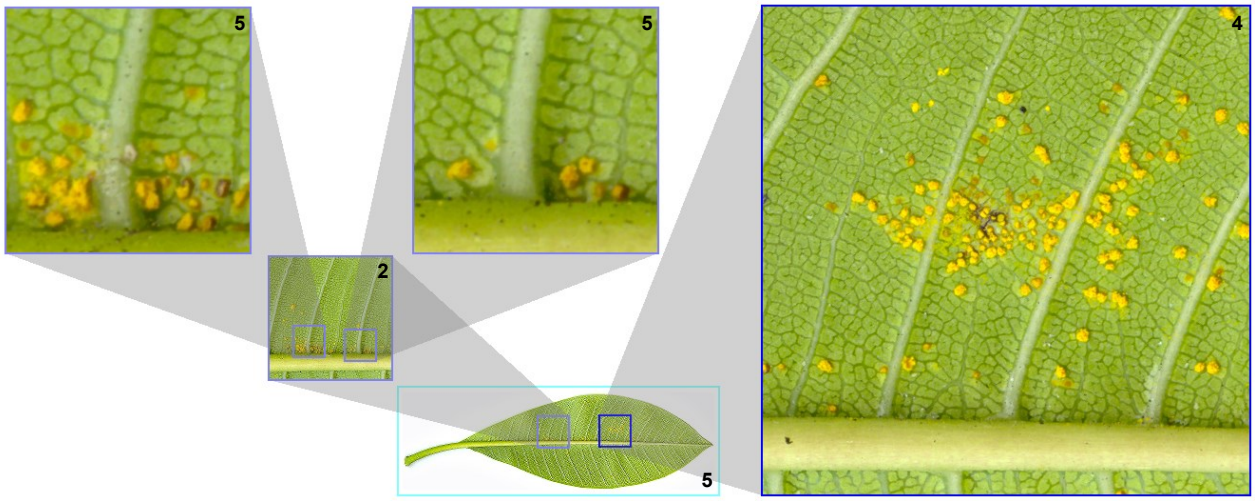

(a) Plumeria rubra leaf with frangipani rust. Source image dimensions: 10496 × 3328

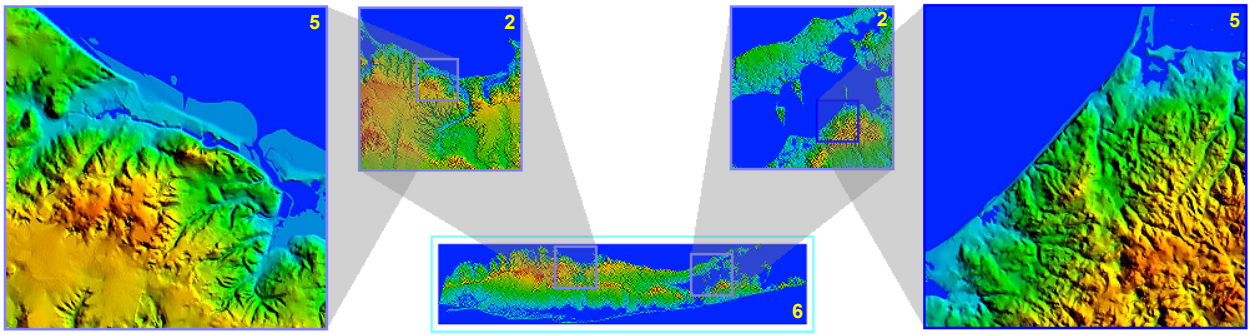

(b) Topographic shading of Long Island. Source image dimensions: 18944 × 4224

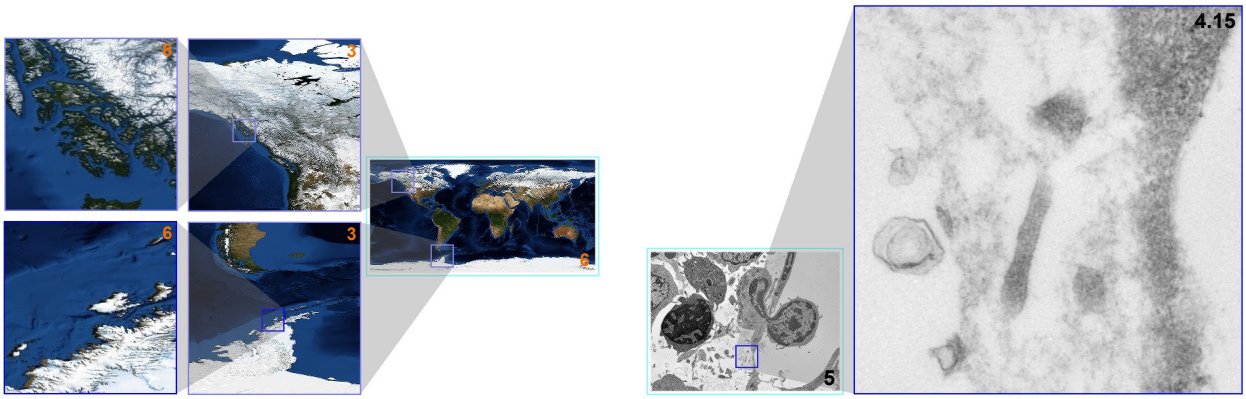

(c) Comparison between the ice near the coasts of the Prince of Wales Island (top) and the Alexander Island (bottom). Source image dimensions: 21632 × 10816

(d) A thin section cut through a bone marrow area near the cartilage/bone interface in a mouse kneecap. Source image dimensions: 9216 × 6784

Fig. 4 Various multilevel focus+context visualization hierarchies for 2D images

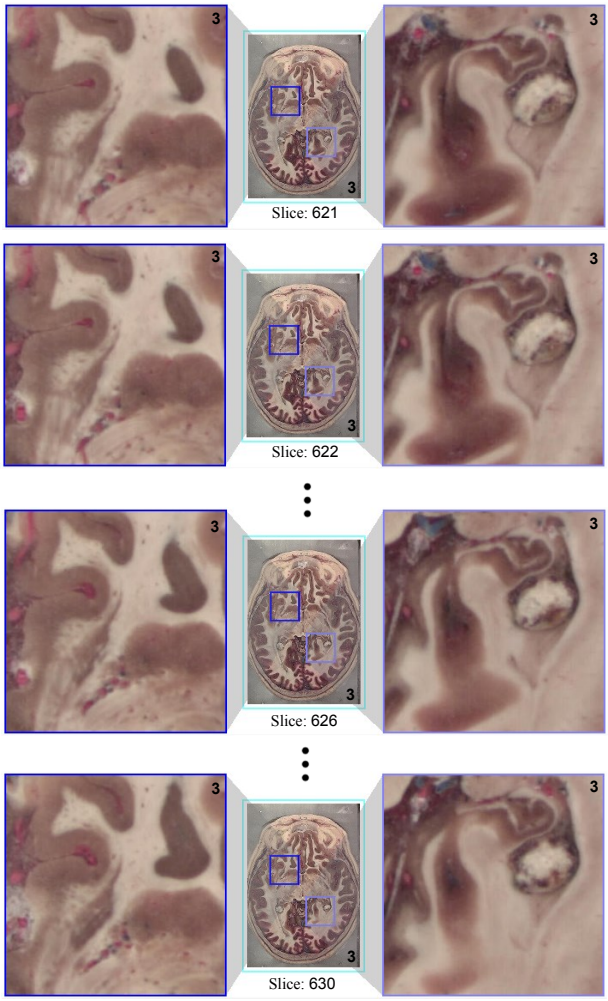

Fig. 5 A fly-through focus+context visualization for a 3D image – part of a male's head. Source image dimensions: $1056 \times 1528 \times 150$

query windows to move back and forth along the time dimension.

6 Performance characteristics

The runtimes for the performed decomposition and reconstruction operations are linear on the number of processed samples. For our implementation, the memory usage is linear on the total number of samples in the source image and the enlarged ROIs.

On a Dell Precision T7500 desktop computer with two Intel® Xeon® E5506 2.13 GHz processors, NVIDIA Quadro FX 1800 graphics card, and 12 GB of RAM, our experiments revealed the average frame rates shown in Table 1. They were obtained during ROI movement for different levels of enlarged ROI resolution. We used the diseased leaf image shown in Fig. 4(a) in these experiments. Each frame rate value in the table is the average of frame rates from three different sets of user interactions (involving only ROI movement), keeping the level of enlarged ROI resolution constant. The second and third columns of the table show the average frames per second (FPS) values achieved with and without the use of L-updating technique during ROI movement, respectively. The last column shows how many times higher the average frame rates are while using our proposed L-updating technique.

Table 1 Average frame rates during ROI movement at different levels of enlarged ROI resolution

Level	FPS_1 (L-updating)	FPS_2 (No L-updating)	FPS_1/FPS_2
2	44.84	40.38	1.11
3	43.24	17.56	2.46
4	20.52	4.62	4.45
5	8.11	1.50	5.41

The functionalities of our presented multilevel focus+context visualization framework is not dependent on the choice of multiresolution filters (see Section 4.1.1). One may choose to use a different set of symmetric/antisymmetric multiresolution filters, which will only affect the balanced decomposition (see Section 4.1.2) and perfect reconstruction (see Section 4.1.3) parts of our presented framework. However, the choice of multiresolution filters will affect the performance. Use of filter vectors with shorter widths will imply faster reconstruction (due to reduced number of multiplications) and consequently, higher frame rate.

See our developed prototype in action at 1x speed (Online Resource 1), where it shows interactive multilevel focus+context visualization of large-scale 2D and 3D images, in addition to that of a set of large-scale time-lapse images. It also shows an example with fractional changes in ROI resolution and performs visual comparison between the smoothness of query window movement (affected by the achieved frame rate) with and without the use of the L-updating technique.

7 Conclusion and future work

In this article, we presented a multilevel focus+context visualization framework for effective and manageable navigation and exploration of large-scale 2D and 3D images. Our presented framework extends the discontinuous and undistorted mode of focus+context visualization based on an underlying BWT, utilized by means of a BMR scheme. The BMR scheme we used is devised based on the local multiresolution filters of quadratic B-spline. Unlike preexisting multiresolution approaches to

focus+context visualization, our use of a BMR scheme facilitates straightforward access to details required for on-demand reconstruction of enlarged ROIs and allows us to avoid the use of extraordinary boundary filters.

We also described an *L-updating* technique that ensures real-time feedback by avoiding redundant reconstruction operations in processing reconstruction queries, triggered by a moving query window defining changing ROIs. Our developed prototype allows real-time exploration of large-scale images through interactive manipulation of the visualization hierarchy. We described the data structure that efficiently supports such user interactions. Finally, we discussed various performance characteristics of our presented multilevel focus+context visualization framework.

With the growth of data size, the increasing depth of a multilevel visualization hierarchy supported by a multilevel focus+context framework may cause user disorientation. To address this issue, an important direction for future work involves augmenting enlarged ROIs with supplementary textual and visual information in order to reduce user disorientation. This direction for future work is also aligned with the *scalability and multilevel hierarchy* challenge identified in [26], that highlights the navigation of deep multilevel hierarchies and identifying optimal resolutions (for ROIs, in our context) as major challenges.

Last but not the least, a more flexible multilevel focus+context visualization framework for large-scale 3D images is achievable through an extension of our developed prototype to support their depthwise balanced decompositions and exploration using 3D ROIs that do not need to be axis-aligned.

Acknowledgements This research received generous support from the *Natural Sciences and Engineering Research Council* (NSERC) of Canada, *Alberta Innovates – Technology Futures* (AITF), *Alberta Enterprise and Advanced Education*, and *Network of Centres of Excellence* (NCE) of Canada in *Graphics, Animation and New Media* (GRAND). We would like to thank Mario Costa Sousa for his insightful discussions and Troy Alderson for his helpful editorial comments.

References

1. Bartels, R., Samavati, F.: Multiresolutions numerically from subdivisions. Computers & Graphics **35**(2), 185–197 (2011). DOI 10.1016/j.cag.2010.12.001
2. Bartels, R.H., Golub, G.H., Samavati, F.F.: Some observations on local least squares. BIT Numerical Mathematics **46**(3), 455–477 (2006). DOI 10.1007/s10543-006-0075-y
3. Card, S.K., Nation, D.: Degree-of-interest trees: A component of an attention-reactive user interface. In: Proceedings of the Working Conference on Advanced Visual Interfaces, AVI '02, pp. 231–245. ACM, New York, USA (2002). DOI 10.1145/1556262.1556300
4. Chaikin, G.M.: An algorithm for high-speed curve generation. Computer Graphics and Image Processing **3**(4), 346–349 (1974). DOI 10.1016/0146-664X(74)90028-8
5. Cohen, M., Brodlie, K.: Focus and context for volume visualization. In: Proceeding of the Theory and Practice of Computer Graphics Conference, pp. 32–39. IEEE (2004). DOI 10.1109/TPCG.2004.1314450
6. Cossalter, M., Mengshoel, O.J., Selker, T.: Multi-focus and multi-level techniques for visualization and analysis of networks with thematic data. In: Proceeding of the SPIE Conference on Visualization and Data Analysis, vol. 8654, pp. 1–15 (2013). DOI 10.1117/12.2005096. 865403
7. Hasan, M., Samavati, F.F., Jacob, C.: Multilevel focus+context visualization using balanced multiresolution. In: Proceedings of the International Conference on Cyberworlds, CW, pp. 145–152. IEEE Computer Society (2014). DOI 10.1109/CW.2014.28
8. Hasan, M., Samavati, F.F., Sousa, M.C.: Balanced multiresolution for symmetric/antisymmetric filters. Graphical Models **78**, 36–59 (2015). DOI 10.1016/J.GMOD.2015.01.001
9. Hauser, H.: Generalizing focus+context visualization. In: G.P. Bonneau, T. Ertl, G. Nielson (eds.) Scientific Visualization: The Visual Extraction of Knowledge from Data, Mathematics and Visualization, pp. 305–327. Springer Berlin Heidelberg (2006). DOI 10.1007/3-540-30790-7_18
10. Hodges, E.R.S.: The Guild handbook of scientific illustration. John Wiley and Sons, Hoboken, NJ, USA (2003)
11. Hsu, W.H., Ma, K.L., Correa, C.: A rendering framework for multiscale views of 3D models. In: Proceedings of the SIGGRAPH Asia Conference, SA, pp. 131:1–131:10. ACM, New York, USA (2011). DOI 10.1145/2024156.2024165
12. Kalkofen, D., Mendez, E., Schmalstieg, D.: Interactive focus and context visualization for augmented reality. In: IEEE/ACM International Symposium on Mixed and Augmented Reality, ISMAR, pp. 191–201. IEEE (2007). DOI 10.1109/ISMAR.2007.4538846
13. LaMar, E., Hamann, B., Joy, K.I.: Multiresolution techniques for interactive texture-based volume visualization. In: Proceedings of the Conference on Visualization, VIS, pp. 355–361. IEEE Computer Society Press, Los Alamitos, CA, USA (1999)
14. Losasso, F., Hoppe, H.: Geometry clipmaps: Terrain rendering using nested regular grids. In: ACM SIGGRAPH Papers, SIGGRAPH, pp. 769–776. ACM, New York, USA (2004). DOI 10.1145/1186562.1015799
15. Mendez, E., Kalkofen, D., Schmalstieg, D.: Interactive context-driven visualization tools for augmented reality. In: IEEE/ACM International Symposium on Mixed and Augmented Reality, ISMAR, pp. 209–218. IEEE (2006). DOI 10.1109/ISMAR.2006.297816
16. Packer, J.F.: Focus+context via snaking paths. Master's thesis, Department of Computer Science, University of Calgary, Calgary, Alberta, Canada (2013). URL http://hdl.handle.net/11023/755
17. Plate, J., Tirtasana, M., Carmona, R., Fröhlich, B.: Octreemizer: A hierarchical approach for interactive roaming through very large volumes. In: Proceedings of the Symposium on Data Visualisation, VISSYM, pp. 53–60. Eurographics Association, Aire-la-Ville, Switzerland (2002). DOI 10.2312/VisSym/VisSym02/053-060
18. Ropinski, T., Viola, I., Biermann, M., Hauser, H., Hinrichs, K.: Multimodal visualization with interactive closeups. In: Proceeding of the Theory and Practice of Computer Graphics Conference, pp. 17–24. Eurographics Association (2009). DOI 10.2312/LocalChapterEvents/TPCG/TPCG09/017-024

19. Samavati, F.F., Bartels, R.H.: Multiresolution curve and surface representation: reversing subdivision rules by least-squares data fitting. Computer Graphics Forum **18**(2), 97–119 (1999). DOI 10.1111/1467-8659.00361
20. Samavati, F.F., Bartels, R.H., Olsen, L.: Local B-spline multiresolution with examples in iris synthesis and volumetric rendering. In: S.N. Yanushkevich, M.L. Gavrilova, P.S.P. Wan, S.N. Srihari (eds.) Image Pattern Recognition: Synthesis and Analysis in Biometrics, *Machine Perception and Artificial Intelligence*, vol. 67, pp. 65–102. World Scientific Publishing (2007). DOI 10.1142/9789812770677_0003
21. Suter, S., Guitian, J.I., Marton, F., Agus, M., Elsener, A., Zollikofer, C., Gopi, M., Gobbetti, E., Pajarola, R.: Interactive multiscale tensor reconstruction for multiresolution volume visualization. IEEE Transactions on Visualization and Computer Graphics **17**(12), 2135–2143 (2011). DOI 10.1109/TVCG.2011.214
22. Taerum, T., Sousa, M.C., Samavati, F.F., Chan, S., Mitchell, J.R.: Real-time super resolution contextual close-up of clinical volumetric data. In: Proceedings of the Joint Eurographics – IEEE VGTC Symposium on Visualization, EuroVis, pp. 347–354. Eurographics Association (2006). DOI 10.2312/VisSym/EuroVis06/347-354
23. Tu, Y., Shen, H.W.: Balloon focus: A seamless multi-focus+context method for treemaps. IEEE Transactions on Visualization and Computer Graphics **14**(6), 1157–1164 (2008). DOI 10.1109/TVCG.2008.114
24. Wang, C., Shen, H.W.: Hierarchical navigation interface: leveraging multiple coordinated views for level-of-detail multiresolution volume rendering of large scientific data sets. In: Proceedings of the International Conference on Information Visualisation, pp. 259–267. IEEE (2005). DOI 10.1109/IV.2005.57
25. Wang, Y.S., Wang, C., Lee, T.Y., Ma, K.L.: Feature-preserving volume data reduction and focus+context visualization. IEEE Transactions on Visualization and Computer Graphics **17**(2), 171–181 (2011). DOI 10.1109/TVCG.2010.34
26. Wong, P.C., Shen, H.W., Johnson, C., Chen, C., Ross, R.B.: The top 10 challenges in extreme-scale visual analytics. IEEE Computer Graphics and Applications **32**(4), 63–67 (2012). DOI 10.1109/MCG.2012.87

Mahmudul Hasan is a PhD candidate in the Department of Computer Science of the University of Calgary, where he received his MSc degree in Computer Science in 2009. He graduated with a BSc degree in Computer Science from the Independent University, Bangladesh (IUB), as a *Summa Cum Laude*, ranking 1st among the graduating class of 170 students from his school in 2005. Mr. Hasan was the *Posters Chair* of the 39th Graphics Interface (GI) conference in 2013 and the *Organizing Co-chair* of the 3rd Workshop on Digital Earth held in Banff, Canada in 2015. His research interests include multiresolution and visualization in computer graphics.

Faramarz F. Samavati is a Professor of Computer Science at the University of Calgary. His research interests include computer graphics, geometric modeling, visualization, and 3D imaging. He has published more than 100 papers, one book, and holds two patents. He is an Associate Editor of Elsevier's Computer & Graphics journal and was a Principal Investigator and a Project Leader of the Network of Centers of Excellence (NCE) of Canada in Graphics, Animation and New Media (GRAND). In the years of 2011 to 2015, he has received five Best Paper Awards, a Digital Alberta Award, a Great Supervisor Award, and a University of Calgary Award that honors his contribution in the development of new technologies and innovations.

Christian Jacob is a Professor of Computer Science at the University of Calgary and is co-appointed at the Department of Biochemistry & Molecular Biology in the Cumming School of Medicine, where he is the Director of Bioinformatics for the Bachelor of Health Sciences program. Dr. Jacob is also the Director of the LINDSAY Virtual Human project. He has written two books on evolutionary computing and natural programming paradigms and has published more than 100 papers. His research interests include evolutionary computing, swarm intelligence, and agent-based modelling and simulation of complex biological systems.